

Supplementary material for: *Mantle conveyor beneath the Tethyan collisional belt*

Becker, T. W. and Faccenna, C., *Earth Planet Sci. Lett.*,

doi:10.1016/j.epsl.2011.08.021, 2011.

Thorsten W. Becker*

Department of Earth Sciences, University of Southern California, Los Angeles, CA

Claudio Faccenna

Dipartimento Scienze Geologiche, Università Roma TRE and IGAG, CNR Rome

1 Methods

The surface mechanical boundary conditions for most of our models are shear stress free (free slip), such that plate velocities are driven self-consistently by density contrasts within the mantle (Ricard and Vigny, 1989). The lithosphere in our models is defined rheologically as a relatively stiff layer from the surface to 100 km depth that is “broken” by weak zones of reduced viscosity, as in previous modeling (e.g. King and Hager, 1990; King et al., 1992; Zhong et al., 2000; Yoshida et al., 2001; Faccenna and Becker, 2010). The location of the weak zones used for most models (Fig. 2A) was assigned for the major plate boundaries following the NUVEL-1 geometry, and, for the case of Asia, located at the boundary of the actively deforming region (e.g. England and Molnar, 2005). All velocities are plotted in an Eurasia fixed reference frame (from a best-fit of the velocities within that plate, which typically show large intraplate deformation), and the core-mantle boundary is set to free-slip.

The numerical solution method is based on the finite element, CitcomS approach (Moresi and Solomatov, 1995; Zhong et al., 2000; Tan et al., 2006) with our minor modifications as discussed in Becker (2006) and Faccenna and Becker (2010).

* Address: Department of Earth Sciences, University of Southern California, MC 0740, 3651 Trousdale Pkwy, Los Angeles, CA 90089-0740, USA. Phone: ++1 (213) 740 8365, Fax: ++1 (213) 740 8801

Email address: twb@usc.edu (Thorsten W. Becker).

We have verified that individual models have converged to a stable velocity solution in the presence of lateral viscosity variations. All results shown here have a mesh resolution of ~ 17 km and ~ 26 km in the horizontal and vertical direction, respectively. Resolution tests indicate that model velocities are stable to within a few percent under successive mesh refinement. The numerical resolution employed is therefore sufficient such that the model uncertainties are mainly due to imperfect knowledge of the input models, such as tomography velocity structure, and not due to computational limitations.

As described in Faccenna and Becker (2010), the instantaneous topographic deflection due to mantle flow (“dynamic topography”) was computed by dividing the radial normal stresses at the surface, as predicted by the flow model, by the product of gravitational acceleration (10 m/s^2) and density contrast between the mantle (density $\rho_m = 3350 \text{ kg/m}^3$) and air over land, and the contrast between mantle and seawater (density $\rho_w = 1020 \text{ kg/m}^3$) over water, a standard approximation. The residual topography to which we compare was inferred from crustal models by correcting the observed topography for the expected isostatic topography given the density and crustal thickness of the model CRUST2.0 (Bassin et al., 2000). All topography estimates have short wavelength structure removed by convolution with a Gaussian smoothing filter of 250 km diameter and are then shown after removal of any region-wide average topography.

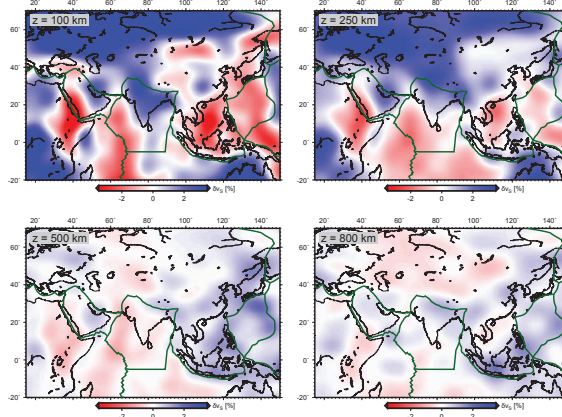
2 Tests with different tomography models

We test the effect of using different seismic tomographic models, as shown in Fig. S1, for inferring mantle density structure and the resulting flow (Figs. S2 and S3). Our reference mantle density model as used for the flow computations shown in Figs. 2 and 3 is based on the global, composite S wave SMEAN model (Becker and Boschi, 2002) (Fig. S1A), with anomalies in the cratonic regions above 250 km removed. Alternative tomography models explored include the upper mantle SV model LH08 (Lebedev and van der Hilst, 2008), merged with SMEAN in the lower mantle (Figs. S1B and S3), and the higher resolution, global P model MITP08 (Li et al., 2008) (Figs. S1C and S2). For LH08, we correct for the presumably depleted nature of cratons by adding positive compositional buoyancy to the otherwise thermally dense (from tomography) regions within cratons.

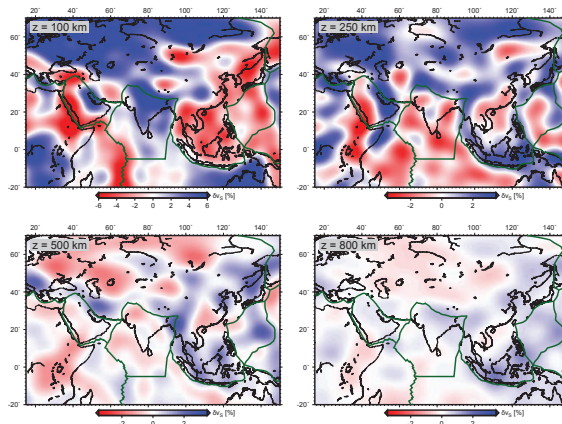
The effect of one particular assumption for lateral variations in viscosity on the flow predictions are shown in Fig. S4, where continental keels down to 250 km (from the 3SMAC mode Nataf and Ricard, 1996) were assigned to be more viscous than the mantle by a factor of 100, and temperature-dependent viscosity was applied elsewhere following the simplified rheological description

$$\eta(T) = \eta_0 \exp(E(T_0 - T)) \quad (1)$$

a) SMEAN



b) LH08_SMEAN



c) MITP08

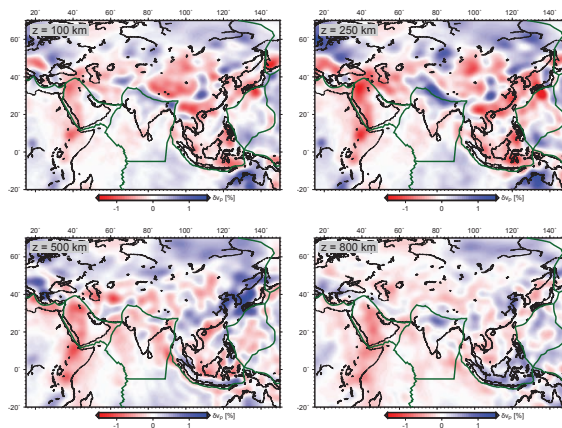


Fig. S1. Comparison of velocity anomaly maps of tomographic models used. A) Reference, global composite *S* wave model, SMEAN (Becker and Boschi, 2002); B) Upper mantle *SV* model LH08 (Lebedev and van der Hilst, 2008), merged with SMEAN in the lower mantle; C) Global, high resolution *P* wave model MITP08 (Li et al., 2008), all shown at 150, 250, 550 and 950 km depths.

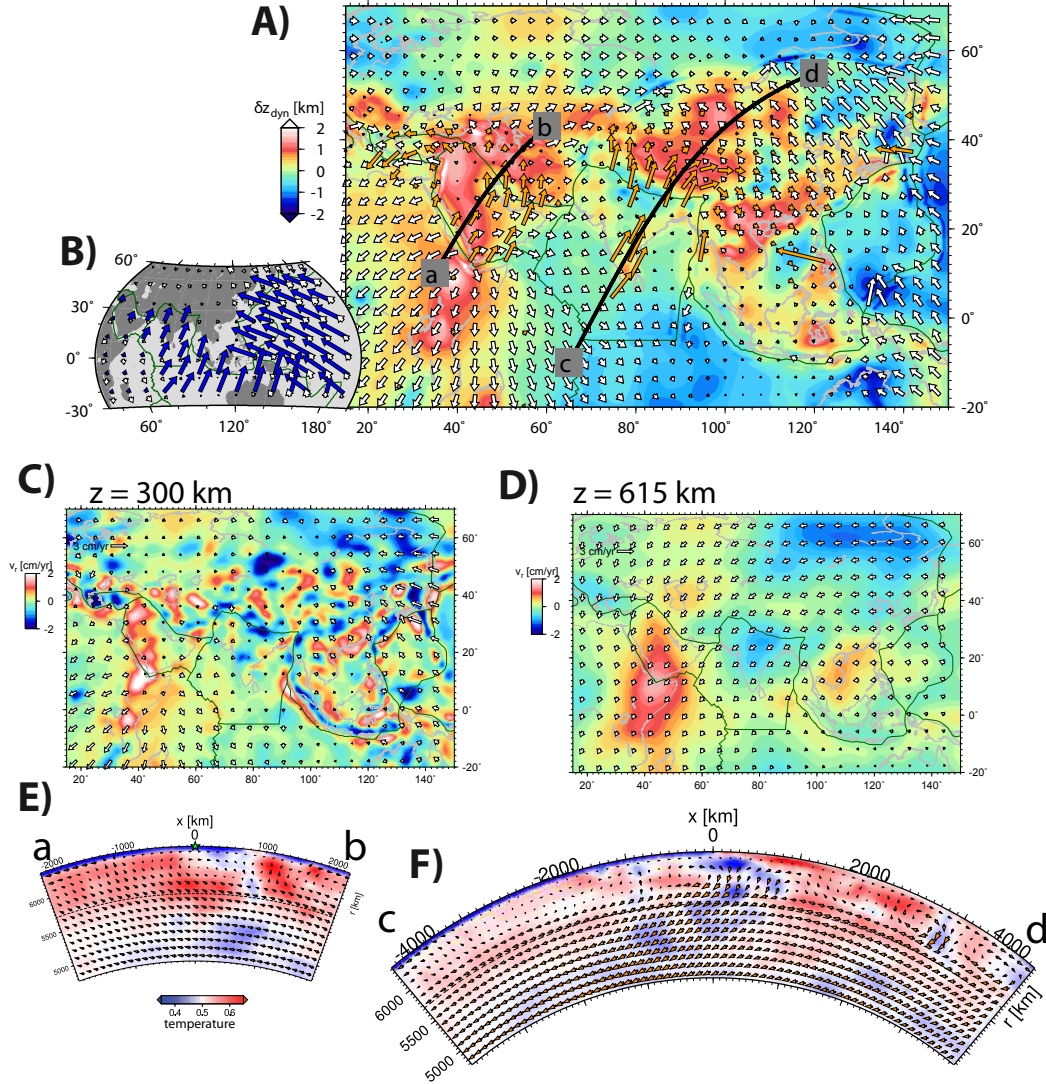


Fig. S2. Additional flow solution based on different tomography, the temperature structure is now inferred from the MITP08 tomography model (Li et al., 2008) (Fig. S1C). A) Predicted surface velocities and dynamic topography (boundary in green) of the Tethyan plate system (white vectors), geodetic velocities (orange), all shown in a best-fit, Eurasia fixed reference frame. B) Global predicted (blue arrows) and observed (white arrows, NUV-EL1A) large-scale velocities; C) Horizontal (white vectors) and vertical flow (background shading) field at 300 km and 615 km depth. Cross-sections from Afar to Iran (E) and from the Carlsberg ridge to Central Asia (F) (trace of cross section as in A), with non-dimensional temperature in the background. Compare with Figs. 2 and 3 in main text.

where η_0 is the mean layer viscosity, T_0 a reference temperature (the mean layer temperature), T the non-dimensional temperature as depicted in the cross-sectional figures and inferred from tomography, and E the Frank-Kaminetskii parameter (here $E = 10$) (see, e.g., Ghosh et al., 2010, for details).

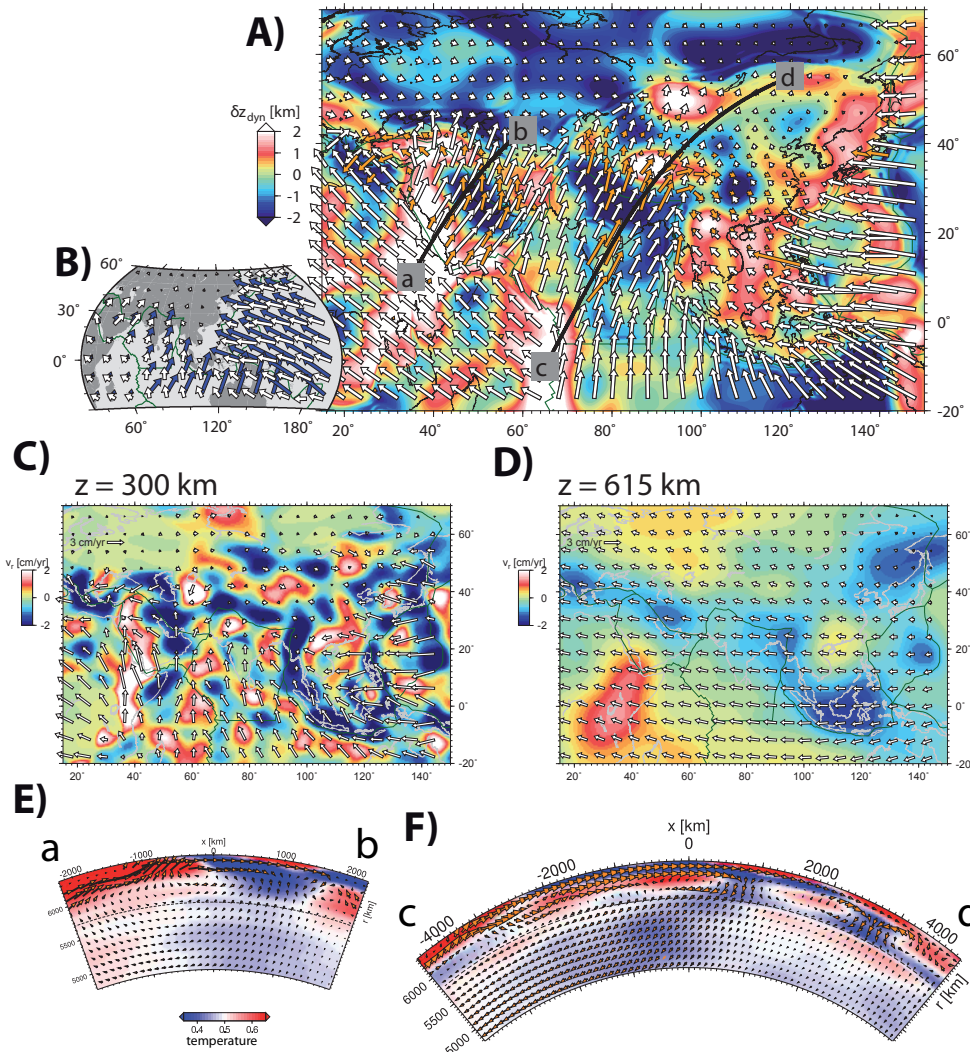


Fig. S3. Additional flow solution based on the *SV* wave tomography model LH08 (Lebedev and van der Hilst, 2008) (Fig. S1B). All plots shown depict the same quantities as in Fig. S2, see there for explanation.

3 Different components of tomography

To test the contributions from different components of the mantle system, we conducted several tests, including partitioning of the tomographic models. Firstly, Fig. S5A shows a more extensive approach in masking out any “cold” contributions underneath the continental lithosphere. There, compositional anomalies might be expected to be erroneously mapped into density by simple scalings of tomographic velocity. The reference model already had cratonic regions from Nataf and Ricard (1996) set to zero above 250 km. By comparing Figs. S5A and Fig. 2C, it can be seen that further removal of negatively buoyant structure in the continental litho-

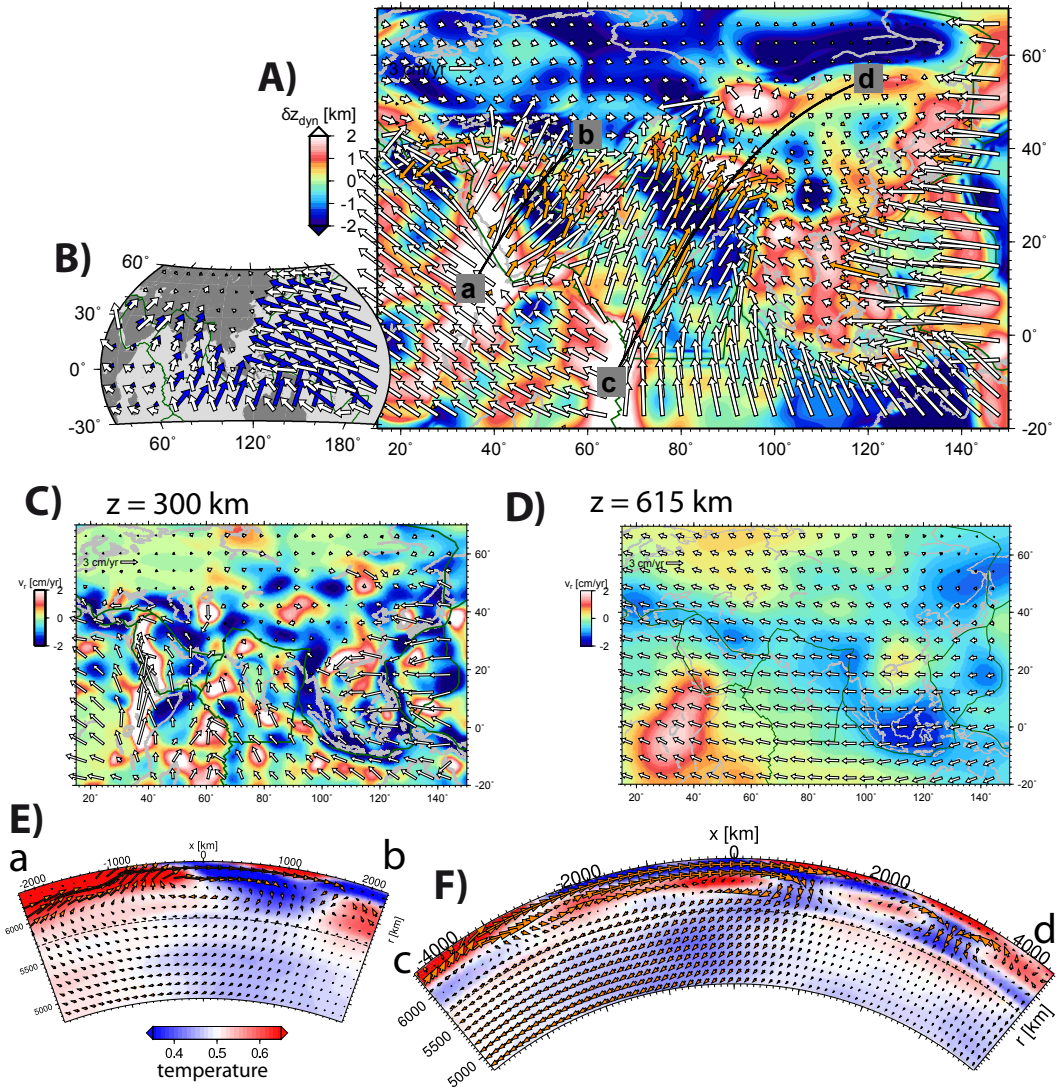


Fig. S4. Additional flow solution for reference model (as in Fig. 2) but including stiff keel beneath cratons and lateral viscosity variations as inferred from temperature (Frank Kaminetskii approximation). All plots shown depict the same quantities as in Fig. S2, see there for explanation.

sphere does not affect the model in a major way. However, the masking of fast, shallow structure does remove some downwellings, such as underneath Arabia and in the immediate vicinity of the India-Eurasia plate boundary. The result is a moderate reduction of India plate motion, to $\sim 80\%$ of the reference when evaluated in the center of the plate.

Secondly, Fig. S5B shows results when all negative (“hot”) anomalies from tomography are removed. Such a test is not equivalent to removing the effect of all upwellings, however. Since our approach does not consider hydrostatic pressure or compressibility effects, only the density anomalies after removal of a layer aver-

age matter for driving flow. This means that relative to any cold anomalies, there are broad regions of relatively hot material, such as underneath most oceanic plates. The resulting effects can be seen, for example, in positive dynamic topography over the spreading-center proximal regions (Fig. S5B). Velocities for India are $\sim 60\%$ of the reference model. Thirdly, flow due to hot anomalies only is shown in Fig. S5C. Plate motions are reduced for the resulting, fairly localized upwellings and very broadly distributed downwellings; India moves at $\sim 35\%$ of the reference model. These results imply that broad-scale upwellings and downwellings are the largest components of the conveyor belt, but localized, active upwellings such as underneath Afar contribute a significant component.

4 Tests with different plate boundaries

Weak zone location, viscosity reduction and width are expected to affect the direction and amplitude of plate motions (e.g. King and Hager, 1990; Zhong et al., 2000; Yoshida et al., 2001). To demonstrate that our general conclusions are independent of those effects and the specific choices of the weak zone geometry used for most models (shown in Fig. 2A), we show surface velocities and dynamic topography for two additional models in Fig. S6. Fig. S6A has the same weak zone geometry as the reference models, but the weak zone thickness is reduced from 300 to 150 km width. Comparison with the reference model shows that predicted dynamic topography and directions of plate motions are very similar for the thin weak zone model, whereas amplitudes of motions, such as for India, are slightly reduced. Fig. S6B uses the same width weak zones as in the reference, but the plate boundaries of Bird (2003) rather than the geologically motivated geometry adopted by us for all other models. Again, dynamic topography is only affected marginally by this change. However, plate motions are modified, particularly in regions where plates are now subdivided into smaller micro-plates, such as Africa and south-east Asia. The motions of Anatolia and India, for example, are sped up in the Bird (2003) plate boundary model, and there is less intraplate deformation in Tibet compared to the reference model. The decoupling of Nubia from Africa leads to overall more easterly trending velocities within India and the Eurasian plate. However, the broad-scale motions are consistent with the reference model and the arguments set forth in the main text.

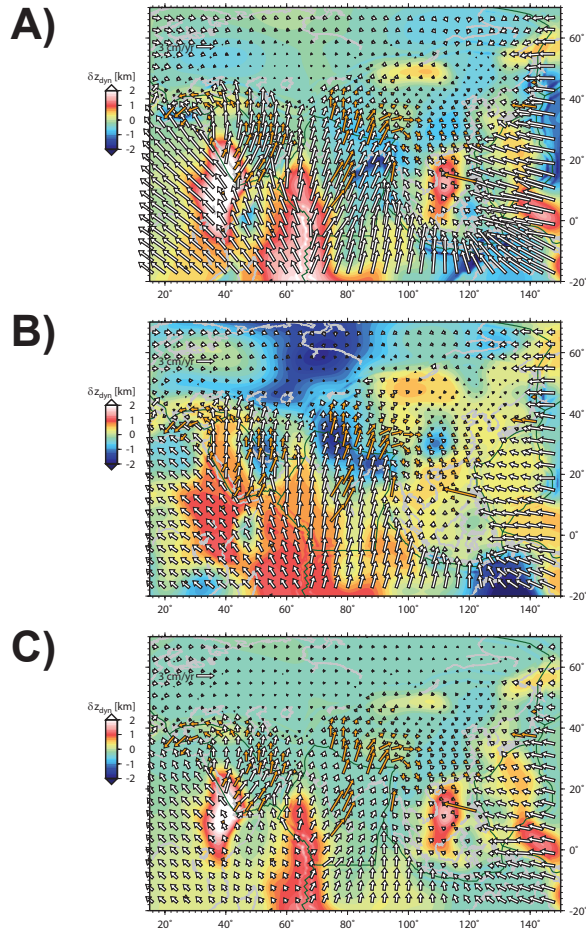


Fig. S5. Additional flow solutions, showing surface velocities and dynamic topography, for the reference model (as in Fig. 2C) but, A), setting positive (“cold”) tomographic velocity anomalies underneath all continental regions (from Nataf and Ricard, 1996) (not just cratons) above 250 km to zero; B) setting all negative (“hot”) velocity anomalies to zero in the tomographic model; and, C), setting all cold anomalies in tomography to zero.

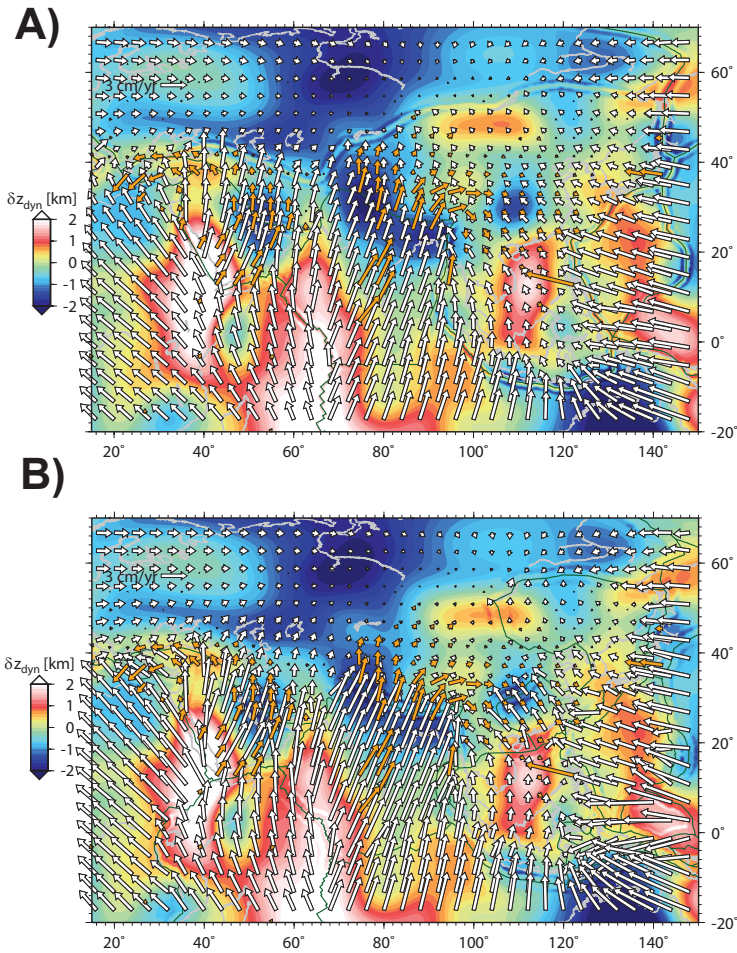


Fig. S6. Additional flow solutions, showing surface velocities and dynamic topography (as in Fig. 2C), for the reference model but, A), using thinner (150 km instead of 300 km wide) weak zones, and, B), using same width weak zones but along the plate boundaries from Bird (2003) instead of the geometry shown in Fig. 2A (see green lines).

References

- Bassin, C., Laske, G., Masters, G., 2000. The current limits of resolution for surface wave tomography in North America (abstract). *Eos Trans. AGU* 81, F897.
- Becker, T. W., 2006. On the effect of temperature and strain-rate dependent viscosity on global mantle flow, net rotation, and plate-driving forces. *Geophys. J. Int.* 167, 943–957.
- Becker, T. W., Boschi, L., 2002. A comparison of tomographic and geodynamic mantle models. *Geochem., Geophys., Geosys.* 3, 1. doi:10.1029/2001GC000168.
- Bird, P., 2003. An updated digital model of plate boundaries. *Geochem., Geophys., Geosys.* 4. doi:10.1029/2001GC000252.
- England, P., Molnar, P., 2005. Late Quaternary to decadal velocity fields in Asia. *J. Geophys. Res.* 110, B12401. doi:10.1029/2004JB003541.
- Faccenna, C., Becker, T. W., 2010. Shaping mobile belts by small-scale convection. *Nature* 465, 602–605.
- Ghosh, A., Becker, T. W., Zhong, S., 2010. Effects of lateral viscosity variations on the geoid. *Geophys. Res. Lett.* 37, L01301. doi:10.1029/2009GL040426.
- King, S. D., Gable, C. W., Weinstein, S. A., 1992. Models of convection-driven tectonic plates: a comparison of methods and results. *Geophys. J. Int.* 109, 481–487.
- King, S. D., Hager, B. H., 1990. The relationship between plate velocity and trench viscosity in Newtonian and power-law subduction calculations. *Geophys. Res. Lett.* 17, 2409–2412.
- Lebedev, S., van der Hilst, R. D., 2008. Global upper-mantle tomography with the automated multimode inversion of surface and S-wave forms. *Geophys. J. Int.* 173, 505–518.
- Li, C., van der Hilst, R. D., Engdahl, E. R., Burdick, S., 2008. A new global model for P wave speed variations in Earth's mantle. *Geochem., Geophys., Geosys.* 9, Q05018. doi:10.1029/2007GC001806.
- Moresi, L. N., Solomatov, V. S., 1995. Numerical investigations of 2D convection with extremely large viscosity variations. *Phys. Fluids* 7, 2154–2162.
- Nataf, H.-C., Ricard, Y., 1996. 3SMAC: An *a priori* tomographic model of the upper mantle based on geophysical modeling. *Phys. Earth Planet. Inter.* 95, 101–122.
- Ricard, Y., Vigny, C., 1989. Mantle dynamics with induced plate tectonics. *J. Geophys. Res.* 94, 17,543–17,559.
- Tan, E., Choi, E., Thoutireddy, P., Gurnis, M., Aivazis, M., 2006. GeoFramework: Coupling multiple models of mantle convection within a computational framework. *Geochem., Geophys., Geosys.* 7. doi:10.1029/2005GC001155.
- Yoshida, M., Honda, S., Kido, M., Iwase, Y., 2001. Numerical simulation for the prediction of the plate motions: effects of lateral viscosity variations in the lithosphere. *Earth Planets Space* 53, 709–721.
- Zhong, S., Zuber, M. T., Moresi, L., Gurnis, M., 2000. Role of temperature-dependent viscosity and surface plates in spherical shell models of mantle con-

vection. J. Geophys. Res. 105, 11,063–11,082.